Available online at www.sciencedirect.com

ScienceDirect

Geochimica et Cosmochimica Acta 167 (2015) 11–26

Geochimica et Cosmochimica Acta

www.elsevier.com/locate/gca

Reduction kinetics of aqueous U(VI) in acidic chloride brines to uraninite by methane, hydrogen or C-graphite under hydrothermal conditions: Implications for the genesis of unconformity-related uranium ore deposits

Maxime Dargent [a,*], Laurent Truche [a,*], Jean Dubessy [a], Gilles Bessaque [a], Hervé Marmier [b]

[a] GeoRessources, UMR 7359 CNRS, Université de Lorraine, Campus Aiguillettes, 54506 Vandœuvre-lès-Nancy, France
[b] LIEC, UMR 7360 CNRS, Université de Lorraine, Campus Aiguillettes, 54506 Vandœuvre-lès-Nancy, France

Received 28 September 2014; accepted in revised form 21 June 2015; available online 27 June 2015

Abstract

The formation of hydrothermal uranium ore deposits involves the reduction of dissolved $U(VI)_{(aq)}$ to uraninite. However, the nature of the reducing agent and the kinetics of such a process are currently unknown. These questions are addressed through dedicated experiments performed under conditions relevant for the genesis of unconformity-related uranium (URU) deposits. We tested the efficiency of the following potential reductants supposed to be involved in the reaction: H_2, CH_4, C-graphite and dissolved Fe(II). Results demonstrate the great efficiency of H_2, CH_4 and C-graphite to reduce $U(VI)_{(aq)}$ into uraninite in acidic chloride brines, unlike dissolved Fe(II). Times needed for H_2 (1.4 bar), CH_4 (2.4 bar) and C-graphite (water/carbon mass ratio = 10) to reduce 1 mM of $U(VI)_{(aq)}$ in an acidic brine (1 m LiCl, pH ≈ 1 fixed by HCl) to uraninite at 200 °C are 12 h, 3 days and 4 months, respectively. The effects of temperature (T) between 100 °C and 200 °C, H_2 partial pressure (0.14, 1.4, and 5.4 bar), salinity (0.1, 1 and 3.2 m LiCl) and pH at 25 °C (0.8 and 3.3) on the reduction rate were also investigated. Results show that increasing temperature and H_2 partial pressure increase the reaction rate, whereas increasing salinity or pH have the reverse effect. The reduction of uranyl to uraninite follows an apparent zero-order with respect to time, whatever the considered electron donor. From the measured rate constants, the following values of activation energy (Ea), depending on the nature of the electron donor, have been derived: $Ea_{C\text{-}graphite} = 155 \pm 3$ kJ mol^{-1}, $Ea_{CH4} = 143 \pm 6$ kJ mol^{-1}, and $Ea_{H2} = 124 \pm 15$ kJ mol^{-1} at $T < 150$ °C and 32 ± 6 kJ mol^{-1} at $T > 150$ °C. An empirical relationship between the reaction rate, the hydrogen partial pressure, the uranyl speciation, and the temperature is also proposed. This allows an estimation of the time of formation of a giant U ore deposit such as McArthur River (Canada). The duration of the mineralizing event is controlled both by the U concentration in the ore-forming fluids and the dynamics of gaseous reductants input, and not by the kinetics of $U(VI)_{(aq)}$ reduction itself. Focused flow of mobile electron donors (H_2, CH_4) along quasi vertical fractured zones into $U(VI)_{(aq)}$-bearing oxidized fluids may explain the large volume and high concentrations of uranium in the URU deposits.

* Corresponding authors at: GeoRessources, UMR 7359 CNRS, Faculté des Sciences et Techniques, Entrée 3B – Campus des Aiguillettes, Université de Lorraine, 54506 Vandœuvre-lès-Nancy, France. Tel.: +33 (0)3 83 68 47 28; fax: +33 (0)3 83 68 47 01 (M. Dargent). Tel.: +33 (0)3 83 68 47 13 (L. Truche).
E-mail address: laurent.truche@univ-lorraine.fr (L. Truche).

http://dx.doi.org/10.1016/j.gca.2015.06.027
0016-7037/

1. INTRODUCTION

Uranium is a redox sensitive element and its accumulation under hydrothermal conditions is a precious indicator of the redox state of fluids and their host rocks (Dubessy et al., 1988; Cuney, 2009). Hydrothermal uranium deposits are the main resources of uranium in the world and account for more than 75% of world uranium production (IAEA, 2009). The formation of these deposits implies: (1) the circulation of hydrothermal fluids of varying temperature and salinity through sedimentary and igneous rocks; (2) uranium transport in a hexavalent $U(VI)_{(aq)}$ form as the uranyl ion (UO_2^{2+}) or its associated complexes, and (3) uranium deposition in a tetravalent U(IV) form as uraninite (UO_2). These issues mean that fluctuations of redox conditions are critical for uranium transport and deposition (Dubessy et al., 1988; Cuney, 2009). The three major types of hydrothermal uranium deposits in terms of uranium tonnage are: (1) Roll front deposits (Finch and Davis, 1985; Cai et al., 2007), (2) Iron Oxide Copper–Gold (IOCG) deposits (Hitzman and Valenta, 2005; Williams et al., 2005; Skirrow and Australia, 2009), (3) unconformity-related uranium (URU) deposits (Hoeve and Sibbald, 1978; Jefferson et al., 2007; Kyser and Cuney, 2008b). URU deposits combine spectacularly high grade and large tonnage (up to 200 kt of pure U with an average grade of 20 wt% U at McArthur River, Canada) and have been extensively studied for genetic and economic aspects.

URU deposits are unique to a restricted number of Proterozoic basins including the Athabasca and Thelon basins of Canada and the Kombolgie Basin of Northern Australia (Jefferson et al., 2007; Kyser and Cuney, 2008b). Uranium mineralization as UO_2, is present at the unconformity between an Archean to Paleoproterozoic crystalline basement and a Paleo- to Mesoproterozoic sandstone cover and frequently associated with basement-rooted graphite-rich faults. Uranium mineralization is surrounded by an illite + sudoite (di-tri-octahehedral Mg-chlorite) ± dravite (Mg-tourmaline) alteration halo. These deposits are thought to have formed from large-scale circulation of basinal brines at temperatures of 120–200 °C that percolated between sedimentary basins and underlying crystalline basement rocks (*e.g.* Hoeve and Sibbald, 1978; Derome et al., 2005; Boiron et al., 2010; Richard et al., 2013a). Analysis of fluid inclusions genetically linked with the uranium mineralization by microthermometry, LA-ICP-MS, synchrotron-SRF and XANES have shown that these brines have salinities of 25–35 wt% NaCl equivalent, with highly variable Na/Ca ratios from NaCl-rich (Na > Ca > Mg > K) to $CaCl_2$-rich (Ca > Mg > Na > K) end-members (Pagel et al., 1980; Kotzer and Kyser, 1995; Derome et al., 2005; Richard et al., 2013b), and with $U(VI)_{(aq)}$ contents up to 600 ppm (Richard et al., 2010, 2012). Solubility measurements of $U(VI)_{(aq)}$ (uranium trioxide: $UO_3(H_2O)_n$) in synthetic NaCl brines as a function of pH at 155 °C and vapor saturation pressure have shown that such Cl-rich brines can only transport such high uranium concentrations under acidic conditions: $pH \leqslant 4$ (Rozsypal, 2009; Richard et al., 2012). Experimental studies by Raman spectroscopy of $U(VI)_{(aq)}$-bearing Cl-rich brines have shown that the speciation of $U(VI)_{(aq)}$ is dominated by uranyl chloride complexes with high Cl numbers in the equatorial plane, ($UO_2Cl_n^{2-n}$ where $n = 4$ or 5) at temperatures relevant to URU deposits (Dargent et al., 2013). The deposition of UO_2 requires the reduction of the uranyl complexes. However, it exists a long-standing debate concerning the nature of the electrons donor (Yeo and Potter, 2010).

Alteration of graphitic metasediments by basinal brines is widespread in the vicinity of URU deposits. This alteration results in partial to complete dissolution with corrosion pits (Wang et al., 1989) and remobilization of graphite along faults (Kyser et al., 1989). Graphite has been invoked as a direct reducing agent based on the observation of UO_2 occurrence at the place where graphite was consumed (*e.g.* Alexandre et al., 2005).

Hoeve and Sibbald (1978) hypothesized that CH_4 was the dominant product of hydrothermal alteration of graphite. Bray et al. (1988) proposed that interaction of basinal brines with sulfide-bearing graphitic metasediments could have produced $CO_2 \pm CH_4 \pm H_2S \pm H_2$ gases. Indeed, traces of reduced gases such as CH_4, C_2H_6, or H_2 were detected by Raman spectroscopy in fluid inclusions from URU deposits (Wilde et al., 1989; Derome et al., 2003a,b, 2005). Hydrogen sulfide, from alteration of sulfide minerals, is also a potential reducing agent of $U(VI)_{(aq)}$ (Spirakis, 1981; Cheney, 1985; Beyer et al., 2010). Therefore, the migration of reducing agents (especially CH_4) has been tentatively suggested since the 80's as a process for the reduction of $U(VI)_{(aq)}$ to $U(IV)_{(aq)}$ and subsequent uranium deposition. The reduction of mobile $U(VI)_{(aq)}$ to sparingly soluble UO_2 induced by Fe(II)-bearing minerals (*e.g.* pyrite, chlorite) has also been proposed (Alexandre et al., 2005; Alexandre and Kyser, 2005; Derome et al., 2005). This reaction is possible in the aqueous phase (Privalov et al., 2003), but it is strongly enhanced in the presence of solid surfaces acting as catalysts (Liger et al., 1999; Jeon et al., 2005).

Hydrogen must also be taken into account as a potential reducing agent at the origin of the formation of URU deposits. Molecular hydrogen, together with oxygen, is known to form as a by-product of water radiolysis induced by U decay at the contact of the mineralization (Kish and Cuney, 1982; Dubessy et al., 1988; Krylova et al., 2002; Lin et al., 2005a,b). Nevertheless, the associated production of oxygen (strong oxidant), causing post-mineralization hematitization, probably prevents any efficient self-induced reduction process at this stage. As there is no evidence of hydrogen presence as a primary reagent, it has thus been overlooked by geologists up to now. However, significant potential hydrogen sources have to be considered in the formation of URU deposits such as hydrothermal alteration of Fe(II)-bearing minerals present in the crystalline bedrock (Hawkes, 1972; Salvi and Williams-Jones, 1997; Sherwood Lollar et al., 2002, 2008), reactions of ferrous minerals with H_2S (Drobner et al., 1990; Wächtershäuser, 1990, 1993; Graham and Ohmoto, 1994; Rickard, 1997), or metamorphism of graphitic rocks (French, 1966; Levinson, 1977; Dubessy, 1984; Connolly and Cesare, 1993).

The nature of the reducing agent and the kinetics of $U(VI)_{(aq)}$ to U(IV) reduction and UO_2 deposition have remained among the least understood aspects in U ore deposits genesis (Jefferson et al., 2007; Kyser and Cuney, 2008b). Currently, experimental studies testing the capability of the reducing agents mentioned above, in conditions of URU deposits genesis, are very limited. Moreover, the kinetics of the associated reduction processes is poorly known. Concerning organic matter, Nakashima et al. (1999) have demonstrated the possible $U(VI)_{(aq)}$ reduction into uraninite at around 200 °C under acidic conditions using three types of lignites having different maturities as reducing agents. In the framework of spent nuclear fuel repository, Ekeroth et al. (2004) have experimentally reduced $U(VI)_{(aq)}$ under high hydrogen pressure (40 bar) in carbonated solutions at T ranging from 74 °C to 100 °C. Recently, an experimental study has been performed by Taylor et al. (2015) showing the ability of $Fe(II)_{aq}$ to reduce U(VI) to U(IV). However experiments have been performed at room temperature and pH 7.2. Using reactive mass transport modeling, Aghbelagh and Yang (2014) have evaluated by two different reactions involving either methane as reducing agent or a decrease of oxygen fugacity for the precipitation of uraninite in a typical URU deposit. They concluded that both mechanisms might precipitate uraninite, but they pointed out that only methane is able to explain the massive precipitation of uraninite around the faulted graphite zone. However, these numerical simulations rely on a limited set of thermodynamic (especially for uranyl-chloride complexes) and kinetic data selected from EQ3/6 database (Wolery, 1992; Raffensperger and Garven, 1995), most of these data do not rely on measured experimental values. Therefore, laboratory experiments are needed to constrain these reactive transport models, and to provide the required thermodynamic and kinetic data sets. This question is specifically addressed in this paper through dedicated experiments.

The present work aims first to test the capability and efficiency of some species mentioned above as geological reducing agents under representative conditions for URU deposits genesis. The electron donors investigated in this experimental study are H_2, CH_4, C-graphite and aqueous Fe(II). In addition, the effects of different parameters (temperature, concentration of reductant, chlorinity and pH) on the reduction rate and mechanism are evaluated, and a rate law involving these parameters is proposed. Finally, the derived kinetic parameters are applied to estimate the time scale of U deposition and the quantity of uraninite precipitated under the conditions of URU deposits formation.

2. EXPERIMENTAL METHODS

2.1. Uranyl chloride solutions

Experimental UO_2^{2+}-bearing solutions were obtained from uranyl acetate powder (99.95% pure from Prolabo). This phase was heated during three days at 500 °C in order to obtain UO_3 powder, which was subsequently dissolved in concentrated HCl (31 wt%) at 150 °C. The solution was evaporated to obtain solid $UO_2Cl_2{\cdot}nH_2O$ and then dissolved in H_2O at room temperature. The $U(VI)_{(aq)}$ concentration in the experimental solution was around 10^{-3} mol kg_w^{-1}. The chloride concentration was adjusted by addition of LiCl (0.1, 1.0, and 3.2 mol kg_w^{-1}). The use of LiCl electrolyte instead of a more representative Na, Ca brine (Derome et al., 2005; Richard et al., 2010), does not induce any change on the uranyl speciation as demonstrated by Dargent (2014) at 150 °C-Psat under acidic conditions ($pH_{25\,°C} = 1$). Therefore the choice of the chloride-bearing electrolyte has no effect on the measured reaction rate under our experimental conditions.

Concerning the experiment carried out with $Fe(II)_{aq}$ as the reducing agent, we added $FeCl_2{\cdot}4H_2O$ (from VWR, 99.9% purity) to provide known amounts of $Fe(II)_{aq}$ in solution. Each solutions was acidified by HCl at 0.1 mol kg_w^{-1} ($pH \leqslant 1$) to avoid uranate precipitation (Rozsypal, 2009). To evaluate the effect of pH on the reduction rate, one experiment was performed at pH 3.3 (as measured at room temperature) by adding known amount of 1 mol kg_w^{-1} NaOH to the uranyl stock solution.

2.2. Reactor design and experimental procedure

The experiments in the presence of gaseous reductants (H_2/CH_4) or aqueous Fe(II) were carried out in a Parr® stirred autoclave (titanium grade 4, internal volume of 450 ml), loaded with 250 mL of aqueous solution for each experiment. The nominal maximum temperature and pressure of the reactor is 300 °C and 100 bars, respectively. The reactor was equipped with several capillary tubings that enable periodic sampling of the experimental fluid to monitor reaction progress, and adjustment of the working pressure to a constant value during each run. The vessel and all internal tubings were fitted with Teflon® liners, so that the solution was not in contact with any metallic parts, avoiding corrosion of titanium or potential catalytic effect of the TiO_2 coating of the vessel. The autoclave was loaded and sealed in a glove box ($[O_2] < 5$ ppm). In addition, an argon flow was bubbled in the filled autoclave during 20 min to remove dissolved O_2. Finally, 3 cycles of Ar injection (50 bar) and flushing were performed to remove the last traces of oxygen prior to heating. Both H_2 and CH_4 were loaded as gaseous mixtures of 90%Ar–10% H_2 and 90%Ar–10% CH_4, respectively.

The Ti autoclave contained a Teflon® bowl together with many additional connections (dip tube, stirring, pressure gauge, etc) that represented potential location for C-graphite adhesion, C-graphite being extremely sticky. In addition, it cannot be removed easily by chemical washing. Therefore, the use of the Ti-autoclave with C-graphite would have induced a long lasting contamination. Thus, the experiments in the presence of C-graphite were performed in individual stainless steel autoclaves (Parr® bombs) fitted with Teflon® bowls (15 ml) that were easier to clean, and that can be replaced at a limited cost. In this case, each measurement corresponds to an individual batch experiment (one Parr bomb per experiments). Graphite powder (particles of 5–10 μm in size) and 10 mL of uranyl chloride stock solution (water/rock mass ratio (W/R_C) equal to 10)

Table 1
Summary of experimental conditions for each run. All of the experiments were conducted with 10^{-3} mol kg_w^{-1} UO_2Cl_2 solution. The pH was fixed initially by adding known amount of HCl or NaOH.

Run	T (°C)	$P(H_2)$ (bar)	[LiCl] (mol kg_w^{-1})	pH at 25 °C	k[a] × 10^3(mol kg_w^{-1} day^{-1})	t_{ind}[b] (day)
Experiments with hydrogen						
#01	200	0	1	0.8	0	nd[c]
#02	200	1.4	1	0.8	2.58	nd
#03	170	1.4	1	0.8	1.38	0.06
#04	170	0.14	1	0.8	0.15	0.01
#05	150	1.4	1	0.8	0.90	0.37
#06	150	1.4	0.1	1.1	0.93	0.21
#07	150	5.4	1	0.8	3.28	0.08
#08	150	0.14	1	0.8	0.09	0.33
#09	150	1.4	3.2	0.54	0.056	0.70
#10	150	1.4	1	3.3	0.11	0.22
#11	140	1.4	1	0.8	0.46	0.88
#12	130	1.4	1	0.8	0.13	2.69
#13	130	1.4	0.1	1.1	0.16	0.04
#14	100	1.4	1	0.8	0	nd
#15	100	1.4	0.1	1.1	0.014	2.46
Run	T (°C)	$P(CH_4)$ (bar)	[LiCl] (mol kg_w^{-1})	pH at 25 °C	k[a] × 10^3(mol kg_w^{-1} day^{-1})	t_{ind}[b] (day)
Experiments with methane						
#16	200	2.4	1	0.8	1.034	0.97
#17	170	2.4	1	0.8	0.076	3.75
#18	150	2.4	1	0.8	0.015	6.10
Run	T (°C)	$mass_{C\text{-}graphite}$ ($W/R_{C\text{-}graphite}$)	[LiCl] (mol kg_w^{-1})	pH at 25 °C	k[a] × 10^3(mol kg_w^{-1} day^{-1})	t_{ind}[b] (day)
Experiments with C-graphite						
#19	250	10	1	0.8	0.35	nd
#20	220	10	1	0.8	0.037	nd
#21	200	10	1	0.8	0.0081	nd
Run	T (°C)	[$FeCl_2$] (mol kg_w^{-1})	[LiCl] (mol kg_w^{-1})	pH at 25 °C	k[a] × 10^3 (mol kg_w^{-1} day^{-1})	t_{ind}[b] (day)
Experiment with Fe(II)						
#22	150	0.1	1	0.8	0	nd

[a] Rate constant.
[b] Lag time or induction period.
[c] No determined.

were loaded in anoxic glove box. Experiments were performed at saturated vapor pressure. At the end of experiments, autoclaves were quenched in cold water. A summary of experimental conditions for each run is given in Table 1.

It is important to note that the Teflon® parts of the autoclaves may contain entrapped atmospheric O_2 in the micro porosity. Thus, to ensure anoxic conditions, all Teflon® bowls and liners were pretreated before the series of experiments with a hydrazine solution (N_2H_4 – 20 ppm) at 200 °C during 24 h. Dissolved and occluded O_2 was removed according to the following reaction:

$$O_{2(gas)} + N_2H_{4(aq)} = 2H_2O_{(liq)} + N_{2(gas)} \quad (1)$$

The reactor and the Teflon® parts were carefully cleaned in the glove box using 1 mol kg_w^{-1} HCl and rinsed with milliQ-water prior to use.

2.3. Sampling and analytical techniques

During each Ti-autoclave experiment, solution samples were periodically taken for dissolved uranium concentration analyses. Each time, 2 separate aliquots were sampled for a total volume of 5 mL. The first aliquot was the purge of the sampling line. The second aliquot was immediately diluted in HNO_3 (2 wt%). After each stainless steel autoclave experiment, solution was centrifuged, filtered (0.2 μm) to remove graphite particles, and immediately diluted in HNO_3 (wt 2%). Analyses for U concentration were performed by ICP-OES with a precision of 5% at the 95% confidence level (detection limit at 5 ppb). The pH values were measured at 25 °C in the remaining undiluted solution.

The total amount of sampled solution (*i.e.*, 11–12 samples of 5 mL volume each) did not exceed 25% of the initial volume of solution. Necessary corrections were made to calculate total amounts of uranium by taking into account the volume of solution sampled and the remaining volume of solution in the reactor at each step. At the end of experiments, the autoclaves were quenched in cold water and opened. Solids were immediately transferred into a glove box, rinsed with Milli-Q water, dried and stored in a glove box before conducting structural and mineralogical analyses by scanning electron microscopy (SEM) and transmission electron microscopy (TEM). Concerning experiments performed in Parr-bombs with C-graphite, each

dissolved uranium concentration measurement corresponded to an individual batch experiment.

3. RESULTS

3.1. Validation of the experimental procedure

To demonstrate the absence of the reactivity of Teflon® vis-a-vis uranyl solutions, a blank experiment was performed at 200 °C with experimental solution (no electron donor) in the titanium autoclave under argon atmosphere. The evolution of $[U]/[U]_0$ ratio versus elapsed time is displayed in Fig. 1 (where $[U]_0$ is the initial U concentration and $[U]$ is the concentration at each sampling step). For comparison, a similar experiment was also performed at 200 °C in the presence of 14 bar Ar-10% H_2 gas mixture (*i.e.* 1.4 bar H_2).

The results of the blank experiment showed that $[U]/[U]_0$ ratio remains constant as a function of time demonstrating that no loss of U from solution occured and that Teflon® and the bulk autoclave were inert under the conditions of this study. In contrast, in the presence of H_2, U concentration in solution decreased below the detection limit (5 ppb) in less than 12 h. At the end of the experiment, a fine black powder was observed in the Teflon® bowl. This powder was analyzed by SEM and TEM. Images showed square bipyramid crystals of 1–10 μm size (Fig. 2a, b). Electron diffraction pattern and EDS analysis of particles (Fig. 2c, d) demonstrated that the solid precipitated in the experiment was pure uraninite, thus demonstrating the reduction of dissolved uranyl to UO_2 by hydrogen. These results validated the experimental procedure used in the present study, and demonstrated that H_2 is an efficient electron donor for $U(VI)_{(aq)}$ reduction. In the following sections, we present a complete kinetic parametric investigation using H_2 as the electron donor. The influence of temperature, reductant concentration, chlorinity and pH on the reduction rate was evaluated using H_2, and subsequently compared punctually with experiments involving methane, C-graphite or Fe(II) as the reducing agents.

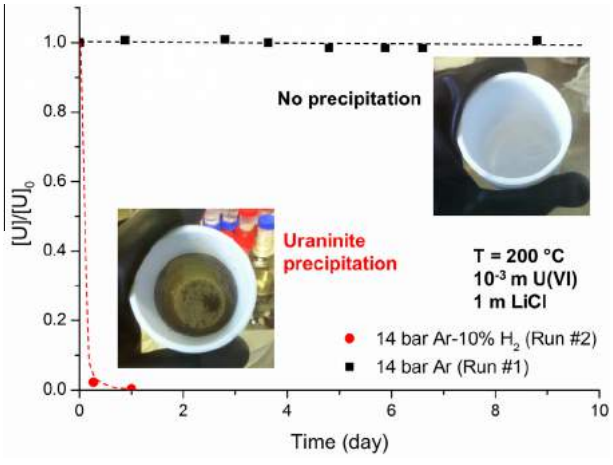

Fig. 1. Comparison of U concentration evolution as a function of time for experiment performed with 14 bar Ar (blank) and with 14 bar Ar-10% H_2. $T = 200$ °C, [LiCl] = 1 mol kg_w^{-1}, and pH = 1 fixed by HCl. Dotted lines are guides for the eyes. Picture in the lower left shows the Teflon bowl in presence of Ar (blank) at the end of experiment without precipitation of solid and picture in the upper right shows precipitation of a fine black powder (uraninite) inside the Teflon bowl fitted to the Ti-autoclave for experiment conducted with H_2.

3.2. Experiments with hydrogen as reducing agent

3.2.1. Effect of temperature

To study the influence of temperature on $U(VI)_{(aq)}$ reduction rate, experiments were performed in the presence of H_2 from 100 °C to 200 °C in 1 m LiCl solution at 14 bar Ar-10% H_2 gas mixture. At temperatures ranging from 130 °C to 200 °C, the $[U]/[U]_0$ ratio rapidly decreased as a function of time (Fig. 3a). Almost 80% of the total U amount in solution was reduced and precipitated in less than 6 h at 200 °C, whereas more than 10 days were required at 130 °C to reach the same reaction yield. At 100 °C, no $U(VI)_{(aq)}$ reduction have been evidenced even after 22 days. Therefore, increasing temperature enhanced the rate of $U(VI)_{(aq)}$ reduction with time. Another important observation was the presence of an initial U concentration plateau prior to the reduction, for experiments conducted at temperatures below 150 °C. The duration of this initial lag time was also dependent upon temperature (*e.g.*, about 24 h at 150 °C and 54 h at 130 °C). At 170 °C and 200 °C, no initial lag time was observed, and after 48 h elapsed time the remaining U concentration in solution was below the ICP-OES detection limit (*i.e.* 5 ppb).

3.2.2. Effect of chlorinity

The influence of chloride concentration on the reduction rate of $U(VI)_{(aq)}$ was investigated for three different chlorinities: 0.1, 1.0 and 3.2 mol kg_w^{-1} LiCl (Fig. 3b). At 150 °C and at 0.1 mol kg_w^{-1} LiCl, 95% of U concentration in solution was reduced in less than 24 h, whereas at 3.2 mol kg_w^{-1} LiCl, only 70% of $U(VI)_{(aq)}$ was reduced after 8 days at the same temperature. The same trend, *i.e.* a decrease of $U(VI)_{(aq)}$ reduction rate with increasing chlorinity, was also observed at 100 °C and 130 °C. For example, the reduction of $U(VI)_{(aq)}$ occurred at 100 °C and 0.1 m LiCl after an initial activation period of 6 days, whereas no reduction was observed at 100 °C and 1 mol kg_w^{-1} LiCl even after 22 days of reaction. The reduction rate of $U(VI)_{(aq)}$ at 100 °C and 0.1 mol kg_w^{-1} LiCl remained very slow (20% $U(VI)_{(aq)}$ reduced in 1 month) compared to the reduction rate at 150 °C or 130 °C for the same chlorinity. It is interesting to note that the duration of the activation period also increased with chlorinity, at 150 °C. Therefore, increasing chloride concentration increased the duration of the activation period and decreased the reduction rate.

3.2.3. Effect of pH

Fig. 3c shows the effect of pH on uranyl reduction rate. At a pH value of 0.8 at room temperature, the reduction of uranyl into uraninite occurred and was completed after 2 days elapsed time at 150 °C, whereas 5 days were required for a total reduction of the same amount of $U(VI)_{(aq)}$ at pH 3.3. Therefore, low pH values increase the reaction rate. In

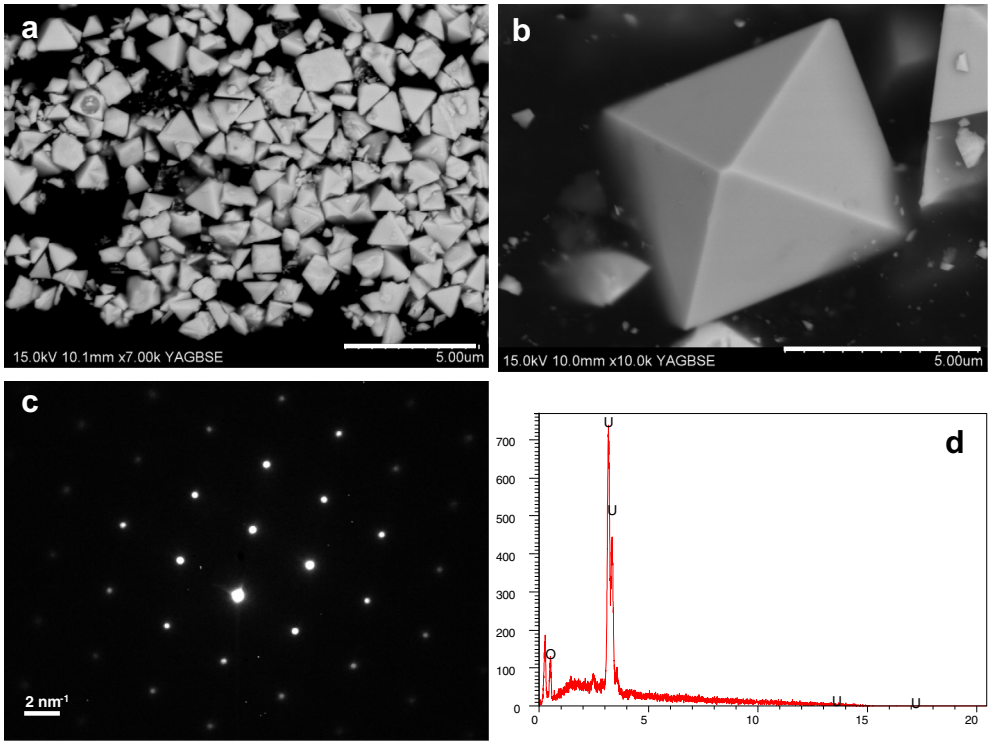

Fig. 2. (a, b) SEM images in backscattered electron mode of uraninite particles precipitated at the end of the experiment Run #2 ($P(H_2) = 1.4$ bar, $T = 200$ °C, [LiCl] = 1 mol kg_w^{-1}, and pH = 1, at room temperature, fixed by HCl). (c) Electron diffraction pattern of (*hkl*) planes of the particles by TEM (d) EDS analysis demonstrate the atomic composition of the particles: 33.33 at.%U, 66.67 at.%O.

order to avoid the precipitation of $U(VI)_{(aq)}$ bearing minerals, no experiments were performed at pH values greater than 3.3. Indeed, the solubility of uranate compounds decreases by 4 orders of magnitude between pH 3 and 4.5 in chloride brines at 150 °C (Rozsypal, 2009; Richard et al., 2012).

3.2.4. Effect of PH_2

The effect of H_2 partial pressure was examined using 3 different pressures (0.14, 1.4 and, 5.4 bar) at 150 °C and at 2 different pressures (0.14 and 1.4 bar) at 170 °C (1 mol kg_w^{-1} LiCl). The amount of $U(VI)_{(aq)}$ reduced to uraninite increased with the increase of H_2 partial pressure as shown in Fig. 3d. Following Henry's law, aqueous H_2 concentration is proportional to PH_2 (9.5×10^{-5}, 9.5×10^{-4} and, 4.8×10^{-3} mol kg_w^{-1} respectively for 0.14, 1.4 and, 5.4 bar at 150 °C), and the observed increase of $U(VI)_{(aq)}$ reduction rate with PH_2 rise was therefore expected.

3.3. Experiments with methane as reducing agent

The reactivity of $U(VI)_{(aq)}$ in the presence of 2.4 bar methane partial pressure (dissolved aqueous CH_4 concentration is 1.9×10^{-3} mol kg_w^{-1} at 200 °C, i.e. similar to H_2 dissolved concentration in H_2-experiments for sake of consistency), was investigated at 150 °C, 170 °C and 200 °C. Results, plotted in Fig. 4a, showed the same trends as those observed in the presence of H_2, *i.e.* the reaction rate increased with temperature. An initial activation period was also observed below 170 °C. However, at comparable dissolved gas concentrations, the reaction rates were lower in the presence of CH_4 compared to H_2. A qualitative analysis of the vapor phase composition by gas chromatography has shown traces of CO_2. This observation points out to a partial oxidation of CH_4 into CO_2, in agreement with the corresponding reduction of $U(VI)_{(aq)}$ to UO_2(s).

3.4. Experiments with C-graphite as reducing agent

Fig. 4b shows the results of experiments in the presence of C-graphite. At 200 °C, only 30% of the dissolved U was reduced after 1 month. For kinetic reasons, experiments in the presence of C-graphite were carried out at higher temperature than for CH_4 and H_2-bearing experiments. Like other electron donors tested in this study, the reaction rate increased with temperature. However, the reaction rate for $U(VI)_{(aq)}$ reduction in the presence of C-graphite was clearly lower than the one measured in the presence of H_2 or CH_4. The slight scattering of the data was likely due to loading and sampling uncertainties (see Section 2.2 above).

3.5. Experiment with dissolved Fe(II) as reducing agent

One experiment was performed in the presence of dissolved Fe(II) (0.1 mol kg_w^{-1} $FeCl_2$) at 150 °C and 1 mol kg_w^{-1} LiCl (Run #22, Table 1). Under such conditions, the speciation of $Fe(II)_{(aq)}$ as calculated with Phreeqc software (V.2.18: Parkurst and Appelo, 1999) using the LLNL database (Johnson et al., 2000) was dominated by three species: the free ion Fe^{2+} (50%), and two iron chloride

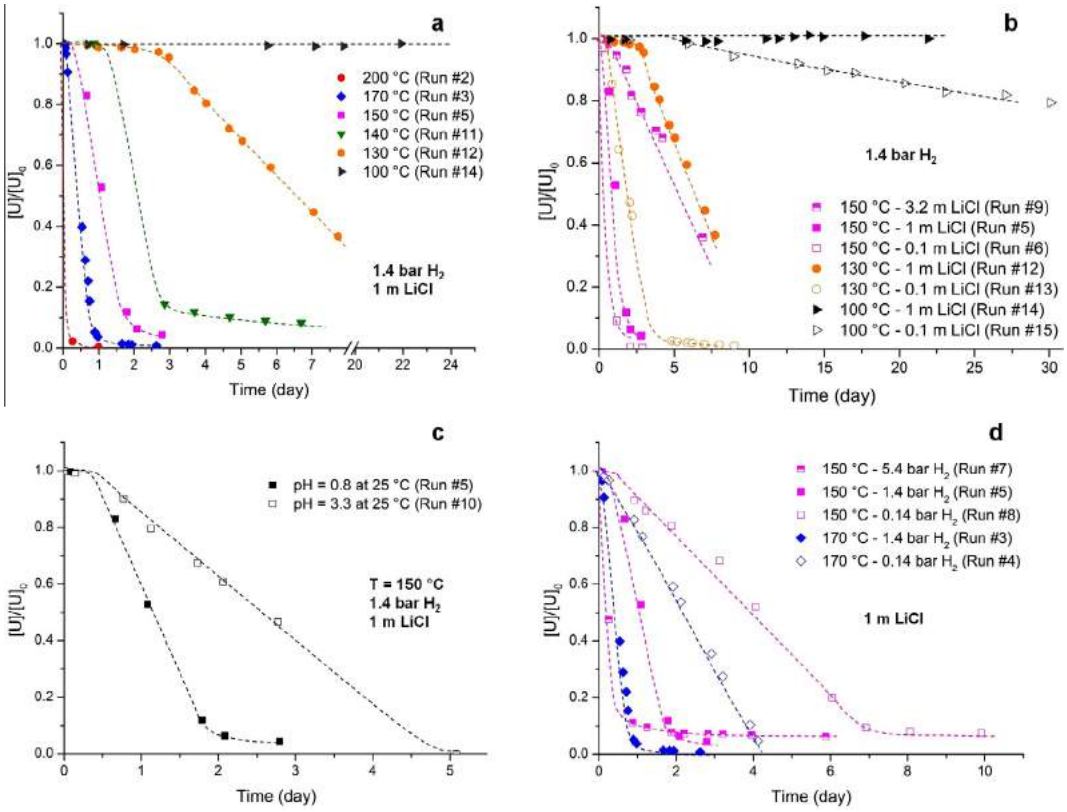

Fig. 3. Effect of temperature (a), chlorinity (b), pH (c) and hydrogen partial pressure (d) on U concentration decrease as a function of time normalized to the initial uranium concentration $[U]_0$. Fixed parameters for each range of experiments are given on Fig. 3. Dotted lines are guides for the eyes.

complexes, $FeCl^+$ (26%) and $FeCl_4^{2-}$ (24%). A constant dissolved U concentration was monitored over 18 days, and no uraninite was recovered at the end of the experiment. Thus Fe^{2+} was not able to reduce $U(VI)_{(aq)}$ in the present experimental conditions. This result was supported by thermodynamic calculations performed with Phreeqc software together with the LLNL database, showing that $U(VI)_{(aq)}$ was not reduced by dissolved Fe^{2+} at 150 °C in acidic brine at pH equal to 1.

4. DISCUSSION

4.1. Efficiency of the tested reducing agents: H_2, CH_4, C-graphite and $Fe(II)_{(aq)}$

The different sets of experiments performed in this study allow a comparison of the efficiency of several electron donors for uranyl reduction in chloride-bearing acidic solution under hydrothermal conditions. Except for $Fe(II)_{(aq)}$, hydrogen, methane and C-graphite appear to be efficient reducing agents for $U(VI)_{(aq)}$ at temperatures representative of URU deposits formation. The redox reactions between uranyl and the different electron donors can be written as:

$$UO^{2+}_{2(aq)} + C_{(s)} + H_2O_{(liq)} = UO_{2(s)} + CO_{(aq)} + 2H^+_{(aq)} \quad (2a)$$

$$2UO^{2+}_{2(aq)} + C_{(s)} + 2H_2O_{(liq)} = 2UO_{2(s)} + CO_{2(aq)} + 4H^+_{(aq)} \quad (2b)$$

$$3UO^{2+}_{2(aq)} + CH_{4(aq)} + H_2O_{(liq)} = 3UO_{2(s)} + CO_{(aq)} + 6H^+_{(aq)} \quad (3a)$$

$$4UO^{2+}_{2(aq)} + CH_{4(aq)} + 2H_2O_{(liq)} = 4UO_{2(s)} + CO_{2(aq)} + 8H^+_{(aq)} \quad (3b)$$

$$UO^{2+}_{2(aq)} + H_{2(aq)} = UO_{2(s)} + 2H^+_{(aq)} \quad (4)$$

The consideration of the reduction potential is a classical and straightforward way to evaluate the direction of spontaneous reactions and the magnitude of the driving force behind them. In our case, it is possible to rank the reactivity of electron donors following their reduction potential in the order $H_2 > CH_4 > C$ with $E(H^+/H_2)$, $E(CO_2/CH_4)$ and $E(CO_2/C)$ being equal to 0.007 V, 0.192 V, and 0.228 V respectively at 200 °C and at saturated vapor pressure (as calculated from the Gibbs free energies of formation at 200 °C and P_{sat} given by Oelkers et al., 1995).

No uranyl reduction has been observed in the presence of dissolved Fe^{2+}, under the same conditions as those tested for the other reducing agents. This result is also in good agreement with the thermodynamic predictions made for uranyl reactivity in the presence of 0.1 mol kg_w^{-1} $Fe(II)_{(aq)}$ at pH 1. Such a conclusion does not preclude the possible reduction of uranyl by ferrous compounds under less acidic conditions. Indeed, thermodynamic calculation indicates that $U(VI)_{(aq)}$ can be reduced into uraninite at pH 3 in the presence of $Fe(II)_{(aq)}$. Such a reaction process requires further experimental investigation.

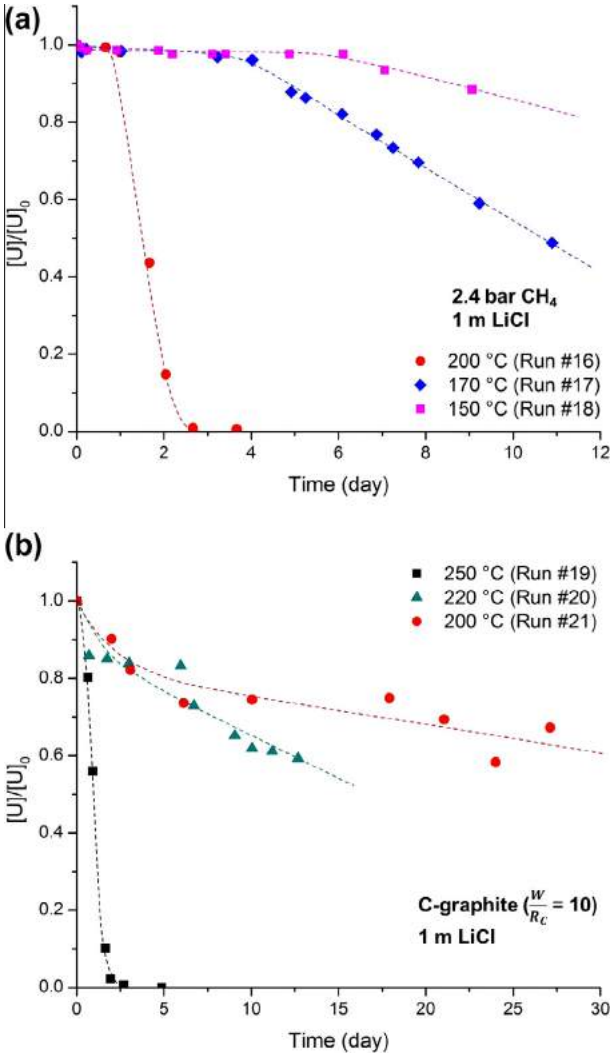

Fig. 4. Effect of temperature on uranyl reduction rate in the presence of: (a) 2.4 bar CH_4, and (b) C-graphite (water/rock mass ratio $\frac{W}{R_C} = 10$). Dotted lines are guides for the eyes.

However, this simple consideration based on thermodynamic data at 200 °C and saturated vapor pressure does not give any information about kinetics or reaction mechanisms (*e.g.* non-equilibrium reaction, presence of multiple redox couples, speciation, interface processes, inert redox couples, temperature, and pH effect). Consequently, the direct use of the reduction potentials as indicator of reaction processes must be done with caution.

After an activation period evidenced in the experiments performed with H_2 and CH_4 (Figs. 3a and 4a), uranyl concentration decreases linearly with time. Therefore, the reduction of uranyl into uraninite follows an apparent zero order rate law with respect to time, whatever the considered electron donor. These zero order rate constants derived from the slope of the regression line corresponding to the linear part of uranium concentration decrease (Figs. 3a and 4a and b) are reported in Table 1.

Fig. 5 compares in an Arrhenius plot our rate measurements for experiments conducted with hydrogen, methane or C-graphite in chloride-bearing aqueous solutions from 100 to 250 °C. Regardless of the temperature and chlorinity, hydrogen is by far the most efficient reducing agent. Uranyl reduction rates measured in the presence of hydrogen and methane are about 2 orders of magnitude higher than those measured in the presence of C-graphite at 200 °C. These results allow ranking the reducing agents efficiency for uranyl reduction in the order: $H_2 > CH_4 >>$ C-graphite, which is in good agreement with the basic reduction potential considerations made previously. This tendency is also reflected by the activation energy values (Ea) of the overall reaction, the lowest energy input required for the reaction to occur being the one measured in the presence of H_2 at $T > 150$ °C. Indeed, the temperature dependence of the rate corresponds to an apparent activation energy of 32 ± 6 kJ mol^{-1} for H_2-experiments, 143 ± 6 kJ mol^{-1} for CH_4-experiments and 155 ± 3 kJ mol^{-1} for C-graphite experiments in the 150–250 °C temperature range. In addition, two different activation energies can be derived for H_2 experiments at 1 m LiCl depending on the temperature regime considered: at T above 150 °C, $Ea = 32 \pm 6$ kJ mol^{-1} and at T below 150 °C, $Ea = 137 \pm 23$ kJ mol^{-1}. This latter activation energy value at T below 150 °C is close to the one found by Ekeroth et al. (2004) at T ranging from 74 to 100 °C (130 kJ mol^{-1}) in carbonate bearing solutions using 40 bar H_2 partial pressure. Ekeroth et al. (2004) have chosen an apparent first order rate law to describe their experimental data. This choice can be debated given the linear relationship between $U(VI)_{(aq)}$ concentration versus time of most of their data. In addition, the initial $U(VI)_{(aq)}$ concentration was 2 orders of magnitude lower in Ekeroth et al. (2004) experiments than in ours: 10^{-5} mol kg$_w^{-1}$ versus 10^{-3} mol kg$_w^{-1}$. Such a low $U(VI)_{(aq)}$ concentration minimizes the collision probability between the reactants, and may

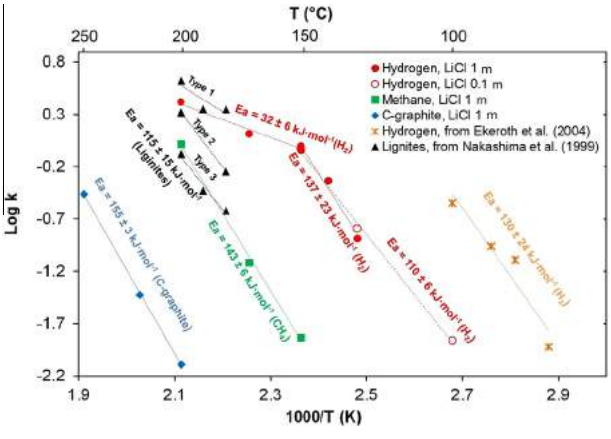

Fig. 5. Arrhenius plot of the inverse of reaction temperature (1000/T with T in Kelvin) versus the decimal logarithm of the rate constant (log k with k in mol kg$_w^{-1}$ day^{-1}) for uranyl reduction in the presence of H_2 (1.4 bar), CH_4 (2.4 bar) and C-graphite (mass ratio $\frac{W}{R_C} = 10$). Comparison with results of Ekeroth et al. (2004) and Nakashima et al. (1999) experiments involving hydrogen and lignite respectively are also shown. Curves represent least square regression.

thus affect the order of the reaction rate. In any case, this wide range of activation energies derived from experiments with H_2, CH_4, and C-graphite as electron donors probably reflects different reaction mechanisms. Therefore, the reaction rate is most likely controlled by the oxidation of the reducing agent and not by the reduction of uranyl into uraninite. Thus, the nature of the electron donor is an important parameter controlling the reaction rate and mechanism. Indeed, H_2 and CH_4 are dissolved species unlike solid C-graphite. Reduction of uranyl by C-graphite involves either a series of steps on the surface by adsorption of $U(VI)_{(aq)}$, or the dissolution of graphite associated with generation of CH_4, H_2, CO and CO_2. In addition, the speciation of $U(VI)_{(aq)}$ may also control the reaction mechanism as demonstrated by the different activation energies measured in presence of H_2 at various temperature range, or at various chlorinity. Indeed, at 1 m LiCl the free uranyl ion UO_2^{2+} predominates in the solution below 150 °C, whereas, the $UO_2Cl_n^{2-n}$ complexes control the uranyl speciation above 150 °C (Dargent et al., 2013). The predominance of $UO_2Cl_n^{2-n}$ complexes above 150 °C probably imposes new steric and energetic constraints for the reaction to occur, and therefore modify the activation energy of the overall reaction. The slow uranyl reduction rate in the presence of C-graphite and CH_4 below 150 °C makes it difficult to derive activation energies in this temperature domain and therefore to confirm the above mentioned effect of uranyl speciation on the reaction mechanism for other electron donor. Concerning the effect of chlorinity, we provide also an estimation of the activation energy at 0.1 mol kg_w^{-1} LiCl in the presence of H_2: $Ea = 110 \pm 6$ kJ mol^{-1}. This later value is slightly lower than the one measured at 1 mol kg_w^{-1} LiCl (137 ± 23 kJ mol^{-1}) indicating the reaction is facilitated at low chlorinity when the speciation of $U(VI)_{(aq)}$ is dominated by the free uranyl ion. The role of uranyl speciation on the reaction mechanism is further discussed below. An average value of activation energy can be given from data below 150 °C in presence of H_2: 124 ± 15 kJ mol^{-1}.

In any case, the reduction rate of uranyl into uraninite induced by hydrogen, or methane, or C-graphite appears to be relatively fast at T above 100 °C, and is probably not a limiting parameter given the geological time scale of the formation of URU ore deposits.

4.2. Reaction kinetics model: experiments with H_2

4.2.1. Reduction rate

The reduction rate of $U(VI)_{(aq)}$ to uraninite increases with temperature and hydrogen partial pressure, but decreases with chlorinity and pH. The plot of the reduction rate k versus PH_2 in log scale suggests a reaction order of 1 with respect to PH_2 (Fig. 6a), which is in agreement with the linear increase of $H_{2(aq)}$ concentration with the increase of hydrogen partial pressure (Henry's law), and the simple H–H bond breaking required for electron transfer between uranyl ion and H_2. Chlorinity is another major factor influencing the reduction rate of uranyl. In Fig. 6b showing the uranyl reduction rate as a function of chlorinity, we superimpose the uranyl speciation as measured by

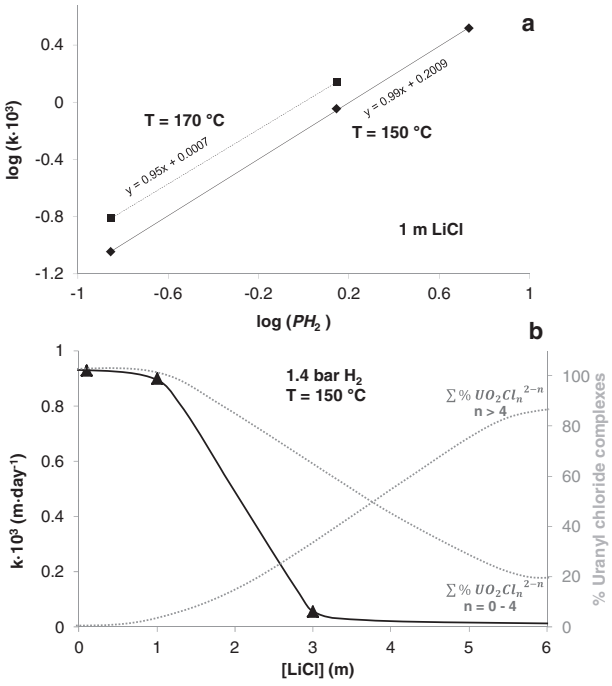

Fig. 6. Variation of the uranyl reduction rate as a function of: (a) $\log P(H_2)$ at 150 °C and 170 °C (curves represent least square regression), and (b) chlorinity in molality scale at 1.4 bar H_2 and 150 °C (Dotted lines are guides for the eyes), Distribution of uranyl chloride complexes is superimposed (Dargent et al., 2013).

Dargent et al. (2013) at 150 °C. At 0.3 mol kg_w^{-1} LiCl and 1 mol kg_w^{-1} LiCl, the uranyl speciation is dominated by a mixture of complexes $UO_2Cl_n^{2-n}$ (n from 0 to 4), whereas at 3.2 m LiCl, the reaction rate decreases drastically with the formation of $UO_2Cl_n^{2-n}$ complexes with n above 4. This suggests that $UO_2Cl_n^{2-n}$ (n from 0 to 4) complexes are more easily reduced than $UO_2Cl_5^{3-}$ and higher chloride ligation number uranyl complexes. This may reflect the high stability of these high chloride number complexes. In addition, it may also reflect some steric constraints imposed by the presence of 4 or 5 chloride ligands in the equatorial plane of the complex, that hamper the electron transfer between UO_2^{2+} and H_2 for $U(VI)_{(aq)}$ reduction. Similarly, at pH 3.3 (Fig. 3c), uranyl hydroxyl complexes are dominant at least at room temperature (Nguyen-Trung et al., 2000). The stability of these complexes at higher temperature could explain the decrease of reaction rate observed with increasing pH. In the absence of experimental data, this question remains open.

In an attempt to determine the rate of uranyl reduction, we fitted our data by an empirical relationship between the reaction rate k (mmol kg_w^{-1} day^{-1}), the hydrogen partial pressure (bar), the activation energy (kJ mol^{-1}), and the contribution (in%, see Fig. 6b) of $UO_2Cl_n^{2-n}$ complexes ($0 \leqslant n \leqslant 4$) for a given chlorinity derived from thermodynamic constants given by Dargent et al. (2013). The rate expression has the form (Eq. (8)):

$$k = a \times \exp\left(\frac{-Ea}{RT}\right) \times (PH_2)^b \times \left(\sum_{n=0}^{4} \%UO_2Cl_n^{2-n}\right)^c \qquad (8)$$

where a is a constant, b and c the reaction orders with respect to hydrogen partial pressure and the contribution of $UO_2Cl_n^{2-n}$ complexes, Ea is the activation energy, R is the gas constant (8.314×10^{-3} kJ mol^{-1} K^{-1}) and T is the temperature in the Kelvin scale. The Gibbs free energy (ΔG) between reactants and products (*i.e.* chemical affinity) does not appear in the rate expression. Indeed, the $(1 - e^{\Delta G/RT})$ term, that appears in the classical expression for the overall rate (k) of an elementary reaction in the Transition State Theory ($k = r_+ (1 - \exp(\Delta G/RT))$ where r_+ stands to the forward reaction rate; *e.g.* Lasaga, 1981), approaches 1 because the solution is far from equilibrium with respect to uraninite under our experimental conditions.

The fitting method was based on non-linear regression of Eq. (8) using XLSAT software. We discriminate two different sets of fitting parameters depending on the temperature range (above or below 150 °C). This choice is justified by the complex evolution of the reaction rate and mechanism as a function of temperature as demonstrated by the change in activation energy and by the influence of uranyl-chloride complexation. The results are gathered in Table 2. Activation energies obtained by fitting are in a good agreement with experimental values. It should be noted that the integration of all variables in the data analysis fits quite well with the values found independently with the consideration of each parameter taken one by one (the plot of the calculated rate constants versus the measured ones is a straight line having a correlation coefficient of 0.98).

4.2.2. Lag time period

The initial lag time period observed in experiments performed with methane or hydrogen (Table 1) can be assimilated to an induction period t_{ind} (day) reflecting the elapsed time required to nucleate the first uraninite crystals (Kashchiev and van Rosmalen, 2003). In the present study, it is assumed that the first crystal formation corresponds to the time at which U concentration starts to decrease. As shown in Fig. 7, log t_{ind}, increases linearly with $1/T$. A relation between induction time and experimental temperature can be applied to determinate the nucleation energy E_{ind} (kJ mol^{-1}) (Lancia et al., 1999):

$$t_{ind} = B \exp\left(\frac{E_{ind}}{RT}\right) \quad (10)$$

where B (day^{-1}) is a constant and R is the ideal gas constant (8.314×10^{-3} kJ mol^{-1} K^{-1}). In log scale, the slope of the linear relation gives indirectly the nucleation activation energy value of 140 ± 3 kJ mol^{-1} at 1.4 bar H_2 and 1 mol kg$_w^{-1}$ LiCl.

Table 2
Fitting parameters for the proposed rate law (Eq. (8)) of $U(VI)_{(aq)}$ reduction by H_2 under acidic conditions (pH ≈ 1) for a given chlorinity (speciation calculations can be done using the stability constants given by Dargent et al. (2013)).

	$T \leqslant 150$ °C	$T \geqslant 150$ °C
Ea (kJ mol^{-1})	110 ± 2	39 ± 3
a	$2.22 \times 10^7 \pm 2 \times 10^6$	2.47 ± 0.50
b	0.95 ± 0.05	0.97 ± 0.05
c	3.08 ± 0.30	2.15 ± 0.50

$k = a \times \exp(\frac{-Ea}{RT}) \times (PH_2)^b \times (\sum_{n=0}^{4} \%UO_2Cl_n^{2-n})^c$ (8).

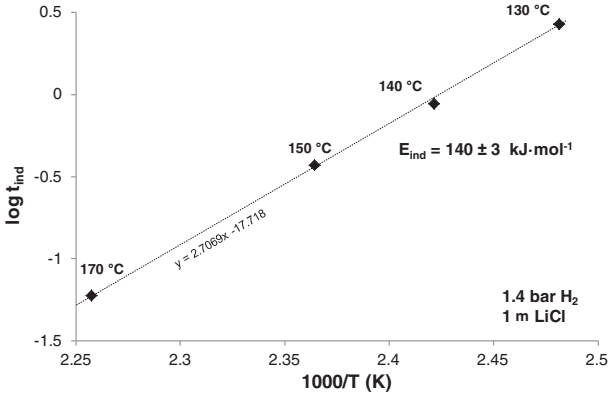

Fig. 7. Arrhenius diagram for uranyl reduction activation period of experiments performed with 1.4 bar H_2 at 1 mol kg$_w^{-1}$ LiCl, and temperature ranging from 130 to 170 °C. The straight line is defined by least square regression.

5. GEOLOGICAL IMPLICATIONS FOR URU GENESIS: CONSTRAINTS ON THE MINERALIZING EVENT

The formation of giant URU ore deposits in relatively short periods of time of 0.1–1 Myr (Raffensperger and Garven, 1995) results from the combination of sustained uranium flux and efficient uraninite precipitation. In the absence of precise geochronological data (Kyser and Cuney, 2008a), calculation of the time necessary to form these massive uraninite orebodies requires the knowledge of numerous parameters, most of them being poorly constrained. The consideration of parameters such as (i) structural setting, (ii) fluid flow rate, (iii) uranium concentration in mineralizing fluid, and (iv) precipitation rate of uraninite, are required to infer the duration of the mineralizing event. In the following discussion we evaluate the time required to form a uranium ore deposit equivalent to McArthur River (Athabasca, Canada), through two different simple *scenarii* corresponding to two possible limiting parameters: either (1) the flux of uranium percolating in a given volume; or (2) the rate of uraninite precipitation considering hydrogen, methane or C-graphite as potential reducing agents.

Scenario #1: the mineralizing event is controlled by the dynamics of uranium input assuming that all the incoming $U(VI)_{(aq)}$ is reduced in a given volume.

Following this scenario, the ore deposition rate can be calculated as a function of (i) uranium concentration in the mineralizing fluid $[U]_0$ (mol kg$_w^{-1}$), (ii) fluid velocity μ (m yr^{-1}), (iii) area of the fluid input section A_{inlet} (m^2), and (iv) the fluid density ρ (kg m^{-3}). It is assumed that the flow of mineralizing fluid is horizontal and unidirectional. The rate law of uranium deposition R_{flux} (ton yr^{-1}) is given by the flux of uranium entering in the mineralization zone:

$$R_{\text{flux}} = [U]_0 \times \mu \times A_{\text{inlet}} \times \rho \times M_U \times 10^{-6} \quad (11)$$

with M_U the molar mass of U (238 g mol^{-1}).

The selected parameters are listed in Table 3 and the results are shown in Fig. 8a for three different uranium concentrations in the mineralizing fluid: 0.1, 1 and 10 ppm. This range of uranium concentration covers the range of uranium content of brines preserved in naturally occurring fluid inclusions from the McArthur River ore deposit (Richard et al., 2010). The calculated times needed to form the McArthur River ore deposit which contained around 192 kt U, are around 0.85 Myr, 8.5 Myr and 85 Myr with ore-forming brines having an uranium concentration of 10, 1 and 0.1 ppm, respectively.

These first-order approximations are in agreement with U–Pb geochronology of primary mineralization giving times range from 50 to 200 Myr in Athasbasca basin (Kyser et al., 2000). This first simple model demonstrates that U concentration in ore-forming fluids is a key parameter to take into account when discussing the kinetic of URU ore genesis. However, the choice of the fluid velocity in this model is also critical. The chosen fluid velocity of 1 m yr^{-1} is an average value for a sandstone layer, but the structural setting of URU deposits can also control the fluid circulation both in terms of flow and direction (Raffensperger and Garven, 1995; Baudemont and Pacquet, 1999). Indeed, for example, the intersections between the graphitic faults and the unconformity can facilitate fluid circulations, increasing the permeability with flow velocity up to 7 m yr^{-1} (Cui et al., 2012). Thus, the calculated duration for the mineralizing event following *scenario #1* may be much shorter (*e.g.* 0.1 Myr with velocity fluid at 7 m yr^{-1} and U concentration in mineralizing fluid at 10 ppm).

Scenario #2: the mineralizing event is controlled by uraninite precipitation rate assuming that the reducing agent supply is not the limiting factor.

As described above, the reduction of uranyl to uraninite by hydrogen, methane or C-graphite follows an apparent zero order rate law with respect of time. Assuming that the concentration of the reductant is constant and supplied in excess with respect to uranyl at the site of deposition, the rate law R_k (ton yr^{-1}) is defined by:

$$R_k = k \times V_{fluid} \times \rho \times M_U \times 10^{-6} \quad (12)$$

with V_{fluid} (m^3) the volume of fluid in the box, which is equal to the porosity times the volume of the box (Table 3). The rate constant k represents moles of U reduced per kilogram of fluid per year. Multiplying k by the number of years, the mass of U-bearing fluid, and converting moles of U to tons, gives the mass of U precipitated in a given number of years. Calculation are performed using the rate constants measured or extrapolated from our experiments at 150 °C and 3.2 mol kg_w^{-1} LiCl with H_2, and at 150 °C and 1 mol kg_w^{-1} LiCl with CH_4 and C-graphite as the reducing agents.

Table 3
Selected parameters for the estimation of duration of the mineralizing event in an URU deposit having the size of McArthur River (Canada).

Box volume[a] (m^3)	450,000
Inlet area (m^2)	9000
Porosity[b]	0.20
Velocity[b] (m y^{-1})	1
Density[b] (kg m^{-3})	2500
Fluid volume in the box (m^3)	90,000

[a] Jefferson et al. (2007).
[b] Cui et al. (2012).

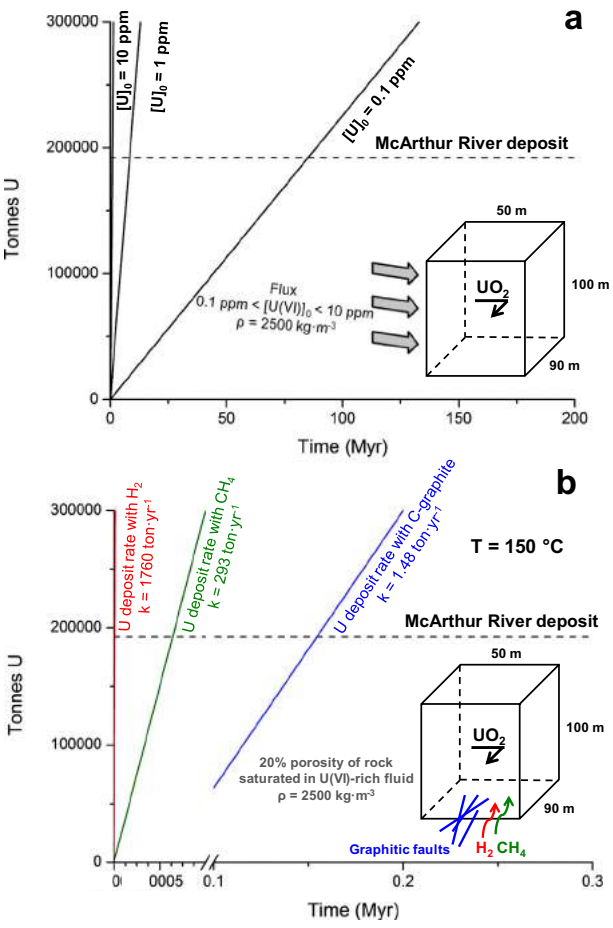

Fig. 8. Tons of U precipitated as a function of time assuming that the mineralizing event is controlled by: (a) the flux of uranium in a given volume with $[U(VI)_{(aq)}]_0$ at 0.1, 1 and 10 ppm in the U-bearing fluid, and (b) by the uranium reduction rate in the presence of 1.4 bar H_2 (3.2 mol kg_w^{-1} LiCl), 2.4 bar CH_4 (1 mol kg_w^{-1} LiCl) and C-graphite (1 mol kg_w^{-1} LiCl) at 150 °C. Rate constants are from Table 3. Tonnage of McArthur River deposit is plotted as an example.

Times obtained to form an ore deposit having the size of Mac Arthur River (192 kt U) are in order of 10 years, 650 years, and 130,000 years respectively with H_2, CH_4, and C-graphite (Fig. 8b), which are a very short duration and, probably, unrealistic period of mineralization time compared to the values calculated following *scenario #1*.

It must be stated that these estimations represent minimum durations applicable to mineralizing fluids having a chlorinity around 1 mol kg_w^{-1} such as those encountered in Northern Australian deposits (Derome et al., 2003b). However, they may be extended by one order of magnitude in fluids having a higher chlorinity such as those of the Athabasca Basin in Canada (up to 9.6 mol kg_w^{-1} chlorinity).

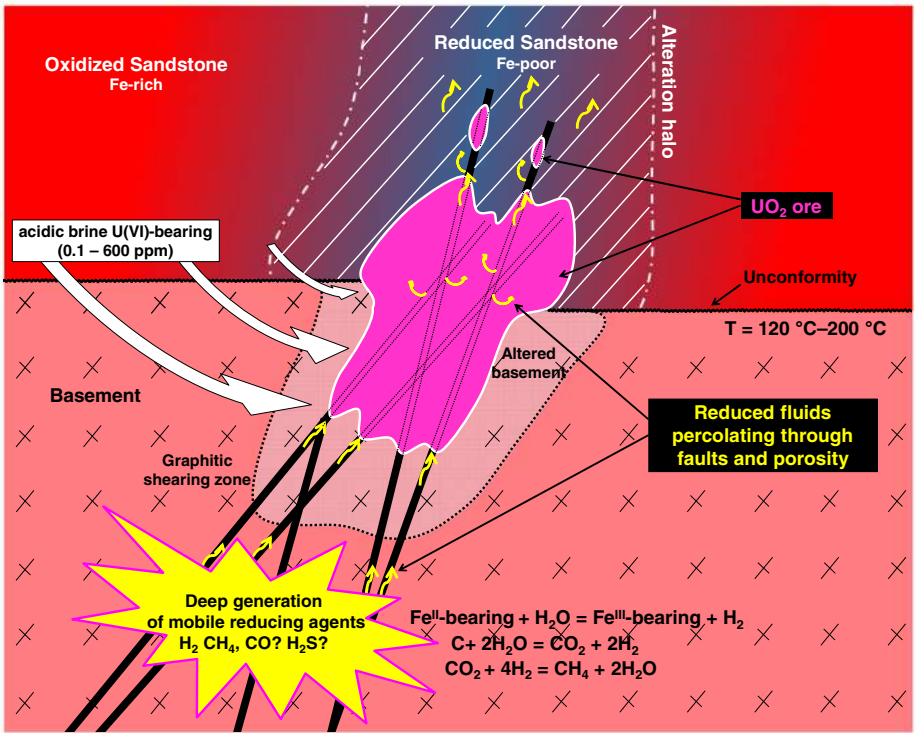

Fig. 9. Schematic representation of a URU deposit genesis involving mixing of $U(VI)_{(aq)}$-bearing brines flowing around the unconformity, with reducing fluid flowing upward from the basement.

These estimations are based on reaction rates obtained under very acidic conditions that are probably well below the expected pH of the mineralizing fluids $3 < pH < 4$, (Richard et al., 2012). However, the reaction rate decreases only by a factor of 8 (Table 1) from $pH_{25\,°C} = 0.8$ ($k = 0.9{\cdot}10^{-3}$ mol kg_w^{-1} day^{-1}) to $pH_{25\,°C} = 3.3$ ($k = 0.11{\cdot}10^{-3}$ mol kg_w^{-1} day^{-1}). Such a weak effect of pH on the reaction rate implies that our estimations remain valid under the expected conditions of URU formation.

In any case, these two boundary scenarii, demonstrate that neither the dynamics of uranium supply nor the kinetics of uranyl reduction are limiting parameters for the ore deposition. All these calculations assume that the reducing agents are continuously supplied at the site of ore deposition, which may not be the case. Although experiments performed in this study attest of graphite efficiency as electron donor, the reduction process of $U(VI)_{(aq)}$ by graphite involves heterogeneous surface reactions which cannot explain alone the massive mineralization characteristics of URU deposits. Moreover, mineralized orebodies are not systematically in contact with graphite and the large alteration haloes surrounding the mineralization is an evidence of syn-ore fluids flowing from the basement upward toward the sandstone cover (Kister et al., 2006).

The trace element chemistry of aluminum-phosphate-sulfate minerals (Gaboreau et al., 2007), the clay mineralogy (ferrous chlorite and illite) and the iron depletion of the sandstone above the mineralization (Bruneton, 1987; Pacquet and Weber, 1993) are evidence for the percolation of a highly reducing fluid driven by the basement-rooted faults and impacting the sedimentary formation far above the unconformity (up to 400 m above). Therefore, the consideration of mobile reducing agents, such as CH_4 or H_2, may explain these observations. The mechanisms of production of reduced fluids carrying H_2 or CH_4 and the way they are supplied to the mineralization site are the key constraints.

Hydrogen is the most efficient investigated reductant. Hydrogen observed in fluid inclusions is interpreted as the product of post-mineralization water radiolysis (Dubessy et al., 1988; Derome et al., 2003a). However, hydrothermal alteration of Fe(II)-bearing minerals in the basement (siderite, chlorite, biotite) into Fe(III)-bearing minerals is also a possible source of H_2 (Berndt et al., 1996; Seyfried Jr. et al., 2007; McCollom and Bach, 2009; Salvi and Williams-Jones, 1997, 2006). Concerning methane, its generation by hydrothermal alteration of graphite was the first hypothesis invoked for the reduction of dissolved $U(VI)_{(aq)}$ to $U(IV)_{(aq)}$ and UO_2 deposition (Hoeve and Sibbald, 1978). The crystalline basement is also a potential source of abiogenetic CH_4 (Sherwood Lollar et al., 1993, 2002, 2006, 2008; Potter et al., 2004; Proskurowski et al., 2008; Taran et al., 2010). Recent investigations have also demonstrated that the occurrences of bitumen in uranium deposits of Athabasca are due to abiogenic synthesis (Sangély et al., 2007). The most widely invoked pathway for the abiogenic formation of methane and other hydrocarbons in geologic environments is the Fischer–Tropsch-type (FTT) synthesis (Salvi and Williams-Jones, 1997; McCollom, 2013 for a review; McCollom and Seewald, 2001).

This study definitely shows that H_2 and CH_4 are efficient as reducing agents due to their reactivity to precipitate $U(VI)_{(aq)}$ and also their high mobility. The mixing of H_2 and CH_4-rich fluids with an $U(VI)_{(aq)}$-rich brine migrating at the unconformity could have triggered uraninite precipitation. The numerous faults deeply rooted in the graphitic metapelites in URU deposits may represent both efficient flow paths for fluids and gases, and important structural constraints for the geometry of the mineralized orebodies (Fig. 9). By this way, the mineralization can be located in the basement (Eagle Point deposit), above the unconformity (McArthur River deposit), or as perched ores (Cigar Lake deposit) depending on the localization of the intersection of the CH_4 or H_2 plume of with the flow of oxidizing U-rich brines percolating around the unconformity (Raffensperger and Garven, 1995; Cui et al., 2012). This model of circulation of mobile and efficient reductants driven by fault systems could be at the origin of the extremely focused and massive character of ore in URU deposits (Fig. 9).

Further investigation of H_2 and CH_4 production both in terms of quantity of generated gas and kinetic, under conditions relevant for URU ore deposit genesis, are required to provide better constraints on the timing of the mineralizing event.

6. CONCLUDING REMARKS

The most important finding from this experimental study are summarized below:

- H_2, CH_4 and C-graphite are efficient reducing agents for dissolved $U(VI)_{(aq)}$ reduction to uraninite in chloride-bearing acidic fluids at temperature ranging from 100 to 250 °C. Dissolved Fe(II) does not reduce $U(VI)_{(aq)}$ under the same conditions.
- The reduction rate of $U(VI)_{(aq)}$ to uraninite increases with temperature and hydrogen partial pressure, but decreases with increasing chlorinity and pH. Uranyl speciation plays an important role on the reaction rate and mechanism.
- Activation energy values (Ea) for dissolved $U(VI)_{(aq)}$ reduction to uraninite derived from our kinetic measurements are the following: $Ea(C\text{-graphite}) = 155 \pm 3$ kJ mol^{-1}, $Ea(CH_4) = 143 \pm 6$ kJ mol^{-1}, $Ea(H_2) = 124 \pm 15$ kJ mol^{-1} at $T < 150$ °C (average value) and 32 ± 6 kJ mol^{-1} at $T > 150$ °C.
- Calculations demonstrate that the duration of the mineralizing event is controlled by the U concentration in the ore-forming fluid and the generation of gaseous reductants rather than by the kinetics of $U(VI)_{(aq)}$ reduction to uraninite.
- As dissolved or gaseous H_2 and CH_4 species, are very mobile electron donors, their mixing with an $U(VI)_{(aq)}$-rich brine migrating at the unconformity could have induced uraninite precipitation. The high mobility of these strong reducing agents coupled with the efficient circulation system driven by graphitic faults deeply rooted in the basement may explain the massive and focused mineralization in URU ore deposits.

Both experimental and field investigations are still needed to better constrain the origin of methane and hydrogen at the conditions of URU deposit genesis. In particular, the potential for hydrogen generation through Fe(II)-bearing minerals hydrothermal alteration and the occurrence of Fischer–Tropsch-type reactions must be carefully assessed.

ACKNOWLEDGMENTS

This work was supported by Labex Ressources 21, CARNOT-ICEEL institute, NEEDS CNRS and AREVA grant. We thank M. Cathelineau, M. Cuney, J. Mercadier and A. Richard for fruitful scientific discussions on URU ore deposits genesis, and C. Nguyen-Trung for his help in preparing the experimental solutions. We appreciate the help of Weihua Liu and one anonymous reviewer for their valuable comments and recommendations on an earlier version of this article, which helped to improve the paper. Dr Gleb Pokrovski is warmly thanked for insightful editorial corrections and very constructive review of the manuscript.

REFERENCES

Aghbelagh Y. B. and Yang J. (2014) Effect of graphite zone in the formation of unconformity-related uranium deposits: Insights from reactive mass transport modeling. *J. Geochem. Explor.* **144**, 12–27, Part A.

Alexandre P. and Kyser T. K. (2005) Effects of cationic substitutions and alteration in uraninite, and implications for the dating of uranium deposits. *Can. Mineral.* **43**, 1005–1017.

Alexandre P., Kyser K., Polito P. and Thomas D. (2005) Alteration mineralogy and stable isotope geochemistry of paleoproterozoic basement-hosted unconformity-type uranium deposits in the Athabasca Basin, Canada. *Econ. Geol.* **100**, 1547–1563.

Baudemont D. and Pacquet A. (1999) The Sue D and E Uranium Deposits, Northern Saskatchewan: Evidence for Structurally Controlled Fluid Circulation in the Athabasca Basin. In *Advances in Saskatchewan Geology and Mineral Exploration*, 14 (eds. K. E. Ashton and C. T. Harper). Sask. Geol. Soc. Spec. Publ., pp. 85–94.

Berndt M. E., Allen D. E. and Seyfried W. E. (1996) Reduction of CO_2 during serpentinization of olivine at 300 °C and 500 bar. *Geology* **24**, 351–354.

Beyer S. R., Kyser K., Hiatt E. E., Fraser I. (2010) Geological evolution and exploration geochemistry of the Boomerang Lake unconformity-type uranium prospect, Northwest Territories, Canada. In *The challenge of finding new mineral resources: global metallogeny, innovative exploration, and new discoveries* (eds. R. J. Goldfarb, E. E. Marsh and T. Monecke). Soc. Econ. Geol. Spec. Publ., 15(2). pp. 675–702.

Bray C. J., Spooner E. T. C. and Longstaffe F. J. (1988) Unconformity-related uranium mineralization, McClean deposits, North Saskatchewan, Canada: hydrogen and oxygen isotope geochemistry. *Can. Mineral.* **26**, 249–268.

Boiron M.-C., Cathelineau M. and Richard A. (2010) Fluid flows and metal deposition near basement/cover unconformity: lessons and analogies from Pb–Zn–F–Ba systems for the understanding of Proterozoic U deposits. *Geofluids* **10**, 270–292.

Bruneton P. (1987) Geology of the Cigar Lake uranium deposit. In *Economic Minerals of Saskatchewan*, 8 (eds. C. F. Gilboy and L. W. Vigrass). Sask. Geol. Soc. Spec. Publ., pp. 99–119.

Cai C., Li H., Qin M., Luo X., Wang F. and Ou G. (2007) Biogenic and petroleum-related ore-forming processes in Dongsheng uranium deposit, NW China. *Ore Geol. Rev.* **32**, 262–274.

Cheney E. S. (1985) Similarities between roll-type and Athabasca unconformity-type uranium deposits and the possible role of sulfides in their origin. In *Geology of Uranium Deposits*, Vol. 32 (eds. T. I. I. Sibbald and W. Petruk), pp. 159–163.

Connolly J. a. D. and Cesare B. (1993) C–O–H–S fluid composition and oxygen fugacity in graphitic metapelites. *J. Metamorph. Geol.* **11**, 379–388.

Cui T., Yang J. and Samson I. M. (2012) Tectonic deformation and fluid flow: implications for the formation of unconformity-related uranium deposits. *Econ. Geol.* **107**, 147–163.

Cuney M. (2009) The extreme diversity of uranium deposits. *Miner. Deposita* **44**, 3–9.

Dargent M. (2014) *Spéciation et réduction de l'U(VI) dans les fluides chlorurés acides en conditions hydrothermales: Du transport au dépôt de l'uranium dans les gisements sous discordance* Ph. D. thesis. Université de Lorraine.

Dargent M., Dubessy J., Truche L., Bazarkina E. F., Nguyen-Trung C. and Robert P. (2013) Experimental study of uranyl(VI) chloride complex formation in acidic LiCl aqueous solutions under hydrothermal conditions ($T = 21$ °C–350 °C, Psat) using Raman spectroscopy. *Eur. J. Mineral.* **25**, 765–775.

Derome D., Cathelineau M., Lhomme T. and Curley M. (2003a) Fluid inclusion evidence of the differential migration of H_2 and O_2 in the McArthur River unconformity-type uranium deposit (Saskatchewan, Canada). Possible role on post-ore modifications of the host rocks. *J. Geochem. Explor.* **78–79**, 525–530.

Derome D., Cuney M., Cathelineau M., Fabre C., Dubessy J., Bruneton P. and Hubert A. (2003b) A detailed fluid inclusion study in silicified breccias from the Kombolgie sandstones (Northern Territory, Australia): inferences for the genesis of middle-Proterozoic unconformity-type uranium deposits. *J. Geochem. Explor.* **80**, 259–275.

Derome D., Cathelineau M., Cuney M., Fabre C., Lhomme T. and Banks D. A. (2005) Mixing of sodic and calcic brines and uranium deposition at McArthur River, Saskatchewan, Canada: a Raman and laser-induced breakdown spectroscopic study of fluid inclusions. *Econ. Geol.* **100**, 1529–1545.

Drobner E., Huber H., Wachtershauser G., Rose D. and Stetter K. O. (1990) Pyrite formation linked with hydrogen evolution under anaerobic conditions. *Nature* **346**, 742–744.

Dubessy J. (1984) Simulation des équilibres chimiques dans le système C–O–H. Conséquences méthodologiques pour les inclusions fluides. *Bull. Minéralogie* **107**, 155–168.

Dubessy J., Pagel M., Beny J.-M., Christensen H., Hickel B., Kosztolanyi C. and Poty B. (1988) Radiolysis evidenced by H_2–O_2 and H_2-bearing fluid inclusions in three uranium deposits. *Geochim. Cosmochim. Acta* **52**, 1155–1167.

Ekeroth E., Jonsson M., Eriksen T. E., Ljungqvist K., Kovács S. and Puigdomenech I. (2004) Reduction of UO_2^{2+} by H_2. *J. Nucl. Mater.* **334**, 35–39.

W.I. Finch, J.F. Davis, Sandstone-type uranium deposits. An introduction. *Geol Environ, Sandstone-Type Uranium Depos IAEA-TECDOC-38 Vienna*. (1985) 11-20.

French B. M. (1966) Some geological implications of equilibrium between graphite and a C-H-O gas phase at high temperatures and pressures. *Rev. Geophys.* **4**, 223–253.

Gaboreau S., Cuney M., Quirt D., Beaufort D., Patrier P. and Mathieu R. (2007) Significance of aluminum phosphate-sulfate minerals associated with U unconformity-type deposits: THE Athabasca basin, Canada. *Am. Mineral.* **92**, 267–280.

Graham U. M. and Ohmoto H. (1994) Experimental study of formation mechanism of hydrothermal pyrite. *Geochim. Cosmochim. Acta* **58**, 2187–2202.

Hawkes H. E. (1972) Free Hydrogen in Genesis of Petroleum: Geological Notes. *AAPG Bull.* **56**, 2268–2270.

Hitzman M. W. and Valenta R. K. (2005) Uranium in Iron Oxide–Copper–Gold (iocg) Systems. *Econ. Geol.* **100**, 1657–1661.

Hoeve J. and Sibbald T. I. I. (1978) On the genesis of Rabbit Lake and other unconformity-type uranium deposits in northern Saskatchewan, Canada. *Econ. Geol.* **73**, 1450–1473.

International Atomic Energy Agency IAEA-TECDOC-1616 (2009) Quantification of Radionuclide Transfer in Terrestrial and Freshwater Environments for Radiological Assessments.

Jefferson C. W., Thomas D. J., Gandhi S. S., Ramaekers P., Delaney G., Brisbin D., Cutts C., Portella P. and Olson R. A. (2007) Unconformity-associated uranium deposits of the Athabasca Basin. In *EXTECH IV: Geology and Uranium EXploration TECHnology of the Proterozoic Athabasca Basin, Saskatchewan and Alberta*, 18 (eds. C. W. Jefferson and G. Delanay). Sask. Geol. Soc. Spec. Publ., pp. 23–67.

Jeon B.-H., Dempsey B. A., Burgos W. D., Barnett M. O. and Roden E. E. (2005) Chemical reduction of U(VI) by Fe(II) at the solid−water interface using natural and synthetic Fe(III) oxides. *Environ. Sci. Technol.* **39**, 5642–5649.

Johnson J., Anderson G. and Parkhurst D. (2000) Database from 'thermo.com.V8.R6.230' prepared by at Lawrence Livermore National Laboratory (Revision: 1.11).

Kashchiev D. and van Rosmalen G. M. (2003) Review: Nucleation in solutions revisited. *Cryst. Res. Technol.* **38**, 555–574.

Kish L. and Cuney M. (1982) Uraninite-albite veins from the Mistamisk Valley of the Labrador Trough, Quebec. *Mineral. Mag.* **44**, 471–483.

Kister P., Laverret E., Quirt D., Cuney M., Patrier Mas. P., Beaufort D. and Bruneton P. (2006) Mineralogy and geochemistry of the host-rock alterations associated with the Shea Creek unconformity-type uranium deposits (Athabasca Basin, Saskatchewan, Canada). Part 2. Regional-Scale Spatial Distribution of the Athabasca group sandstone matrix minerals. *Clays Clay Miner.* **54**, 295–313.

Kotzer T. G. and Kyser T. K. (1995) Petrogenesis of the Proterozoic Athabasca Basin, northern Saskatchewan, Canada, and its relation to diagenesis, hydrothermal uranium mineralization and paleohydrogeology. *Chem. Geol.* **120**, 45–89.

Krylova T. L., Aleshin A. P., Velichkin V. I., Cuney M., Pironon J., Chabiron A. and Poty B. (2002) Uranium-bearing fluid composition at the Streltsovskoye and Antei deposits (Eastern Transbaikalia, Russia). In *Uranium deposits, International workshop* (eds. B. Kribek and J. Zeman). pp. 69–72.

Kyser K. and Cuney M. (2008a) Geochemical characteristics of uranium and analytical methodologies. In *Recent and Not-So-Recent Developments in Uranium Deposits and Implications for Exploration* (eds. M. Cuney and K. Kyser). Mineralogical Association of Canada Short Course Series 39. pp. 23–55.

Kyser K. and Cuney M. (2008b) Unconformity-related uranium deposits. In *Recent and Not-So-Recent Developments in Uranium Deposits and Implications for Exploration*, 39 (eds. M. Cuney and K. Kyser). Mineralogical Association of Canada Short Course Series, pp. 161–219.

Kyser T. K., Wilson M. R. and Ruhrmann G. (1989) Stable isotope constraints on the role of graphite in the genesis of unconformity-type uranium deposits. *Can. J. Earth Sci.* **26**, 490–498.

Kyser K., Hiatt E., Renac C., Duroche K., Holk G. and Deckart K. (2000) Diagenetic fluids in paleo- and meso-Proterozoic sedimentary basins and their implications for long protracted fluid histories. In *Short Course Handbook 28*. Mineralogical Association of Canada, Ottawa, pp. 225–262.

Lancia A., Musmarra D. and Prisciandaro M. (1999) Measuring induction period for calcium sulfate dihydrate precipitation. *AIChE J.* **45**, 390–397.

Lasaga A. C. (1981) Transition state theory. *Rev. Mineral.* **8**, 135–169.

Levinson A. A. (1977) Hydrogen—a reducing agent in some uranium deposits. *Can. J. Earth Sci.* **14**, 2679–2681.

Liger E., Charlet L. and Van Cappellen P. (1999) Surface catalysis of uranium(VI) reduction by iron(II). *Geochim. Cosmochim. Acta* **63**, 2939–2955.

Lin L.-H., Hall J., Lippmann-Pipke J., Ward J. A., Sherwood Lollar. B., DeFlaun M., Rothmel R., Moser D. P., Gihring T. M., Mislowack B. J. and Onstott T. C. (2005a) Radiolytic H_2 in the continental crust: nuclear power for deep subsurface microbial communities. *Geochem. Geophys. Geosyst.* **6**, Q07003.

Lin L.-H., Slater G. F., Sherwood Lollar B., Lacrampe-Couloume G. and Onstott T. C. (2005b) The yield and isotopic composition of radiolytic H_2, a potential energy source for the deep subsurface biosphere. *Geochim. Cosmochim. Acta* **69**, 893–903.

McCollom T. M. and Bach W. (2009) Thermodynamic constraints on hydrogen generation during serpentinization of ultramafic rocks. *Geochim. Cosmochim. Acta* **73**, 856–875.

McCollom T. M. (2013) Laboratory simulation of abiotic hydrocarbon formation in Earth's deep subsurface. *Rev. Mineral. Geochem.* **75**, 467–494.

McCollom T. M. and Seewald J. S. (2001) A reassessment of the potential for reduction of dissolved CO_2 to hydrocarbons during serpentinization of olivine. *Geochim. Cosmochim. Acta* **65**, 3769–3778.

Nakashima S., Disnar J.-R. and Perruchot A. (1999) Precipitation kinetics of uranium by sedimentary organic matter under diagenetic and hydrothermal conditions. *Econ. Geol.* **94**, 993–1006.

Nguyen-Trung C., Palmer D. A., Begun G. M., Peiffert C. and Mesmer R. E. (2000) Aqueous Uranyl Complexes 1. Raman Spectroscopic Study of the Hydrolysis of Uranyl(VI) in Solutions of Trifluoromethanesulfonic Acid and/or Tetramethylammonium Hydroxide at 25 °C and 0.1 MPa. *J. Solutions Chem.* **29**, 101–129.

Oelkers E. H., Helgeson H. C., Shock E. L., Sverjenski D. A., Johnson J. W. and Pokrovskii V. A. (1995) Summary of apparent standard partial molal bibbs free energies of formation of aqueous species, minerals, and gases at pressures 1 to 5000 bars and temperatures 25 to 1000 °C. *J. Phys. Chem. Ref. Data* **24**, 1401.

Pacquet A. and Weber F. (1993) Petrography and mineralogy of alteration halos around the Cigar Lake deposit and their relation to the mineralization. *Can. J. Earth Sci.* **30**, 674–688.

Pagel M., Poty B. and Sheppard S. M. F. (1980) Contribution to some Saskatchewan uranium deposits mainly from fluid inclusion and isotopic data. In *International Uranium Symposium on the Pine Creek Geosyncline* (eds. J. Ferguson and A. Goleby). IAEA, Vienna, pp. 639–654.

Parkurst D. L. and Appelo C. A. J. (1999) User's guide to PHREEQC (version 2). A computer program for speciation, batch-reaction, one-dimensional transport, and inverse geochemical calculations. USGS (Ed.), Water resources investigations report, Denver, CO, USA. pp 99–4259.

Potter J., Rankin A. H. and Treloar P. J. (2004) Abiogenic Fischer–Tropsch synthesis of hydrocarbons in alkaline igneous rocks; fluid inclusion, textural and isotopic evidence from the Lovozero complex, N.W Russia. *Lithos* **75**, 311–330.

Privalov T., Schimmelpfennig B., Wahlgren U. and Grenthe I. (2003) Reduction of Uranyl(VI) by Iron(II) in Solutions: an Ab Initio Study. *J. Phys. Chem. A* **107**, 587–592.

Proskurowski G., Lilley M. D., Seewald J. S., Früh-Green G. L., Olson E. J., Lupton J. E., Sylva S. P. and Kelley D. S. (2008) Abiogenic hydrocarbon production at Lost City hydrothermal field. *Science* **319**, 604–607.

Raffensperger J. P. and Garven G. (1995) The formation of unconformity-type uranium ore deposits 2. Coupled hydrochemical modeling. *Am. J. Sci.* **295**, 639–696.

Rickard D. (1997) Kinetics of pyrite formation by the H_2S oxidation of iron (II) monosulfide in aqueous solution between 25 and 125 °C: the rate equation. *Geochim. Cosmochim. Acta* **61**, 115–134.

Richard A., Pettke T., Cathelineau M., Boiron M.-C., Mercadier J., Cuney M. and Derome D. (2010) Brine–rock interaction in the Athabasca basement (McArthur River U deposit, Canada): consequences for fluid chemistry and uranium uptake. *Terra Nova* **22**, 303–308.

Richard A., Boulvais P., Mercadier J., Boiron M.-C., Cathelineau M., Cuney M. and France-Lanord C. (2013a) From evaporated seawater to uranium-mineralizing brines: isotopic and trace element study of quartz–dolomite veins in the Athabasca system. *Geochim. Cosmochim. Acta* **113**, 38–59.

Richard A., Cauzid J., Cathelineau M., Boiron M.-C., Mercadier J. and Cuney M. (2013b) Synchrotron XRF and XANES investigation of uranium speciation and element distribution in fluid inclusions from unconformity-related uranium deposits. *Geofluids* **13**, 101–111.

Richard A., Rozsypal C., Mercadier J., Banks D. A., Cuney M., Boiron M.-C. and Cathelineau M. (2012) Giant uranium deposits formed from exceptionally uranium-rich acidic brines. *Nat. Geosci.* **5**, 142–146.

Rozsypal C. (2009) Etude expérimentale et modélisation, en fonction du pH et de la concentration en NaCl, du système ternaire U(VI)-NaCl-H_2O à $T = 155$ °C et pression de vapeur saturante. Ph. D. thesis, Université Nancy 1.

Salvi S. and Williams-Jones A. E. (1997) Fischer-Tropsch synthesis of hydrocarbons during sub-solidus alteration of the Strange Lake peralkaline granite, Quebec/Labrador, Canada. *Geochim. Cosmochim. Acta* **61**, 83–99.

Salvi S. and Williams-Jones A. E. (2006) Alteration, HFSE mineralisation and hydrocarbon formation in peralkaline systems: insights from the Strange Lake pluton, Canada. *Lithos* **91**, 19–34.

Sangély L., Chaussidon M., Michels R., Brouand M., Cuney M., Huault V. and Landais P. (2007) Micrometer scale carbon isotopic study of bitumen associated with Athabasca uranium deposits: Constraints on the genetic relationship with petroleum source-rocks and the abiogenic origin hypothesis. *Earth Planet. Sci. Lett.* **258**, 378–396.

Seyfried, Jr., W. E., Foustoukos D. I. and Fu Q. (2007) Redox evolution and mass transfer during serpentinization: An experimental and theoretical study at 200 °C, 500 bar with implications for ultramafic-hosted hydrothermal systems at Mid-Ocean Ridges. *Geochim. Cosmochim. Acta* **71**, 3872–3886.

Sherwood Lollar B., Frape S. K., Weise S. M., Fritz P., Macko S. A. and Welhan J. A. (1993) Abiogenic methanogenesis in crystalline rocks. *Geochim. Cosmochim. Acta* **57**, 5087–5097.

Sherwood Lollar . B., Westgate T. D., Ward J. A., Slater G. F. and Lacrampe-Couloume G. (2002) Abiogenic formation of alkanes in the Earth's crust as a minor source for global hydrocarbon reservoirs. *Nature* **416**, 522–524.

Sherwood Lollar B., Lacrampe-Couloume G., Slater G. F., Ward J., Moser D. P., Gihring T. M., Lin L.-H. and Onstott T. C. (2006) Unravelling abiogenic and biogenic sources of methane in the Earth's deep subsurface. *Chem. Geol.* **226**, 328–339.

Sherwood Lollar B., Lacrampe-Couloume G., Voglesonger K., Onstott T. C., Pratt L. M. and Slater G. F. (2008) Isotopic signatures of CH_4 and higher hydrocarbon gases from Precambrian Shield sites: a model for abiogenic polymerization of hydrocarbons. *Geochim. Cosmochim. Acta* **72**, 4778–4795.

Skirrow R. G. and Australia G. (2009) Uranium mineral systems: processes exploration criteria and a new deposit framework. *Geoscience Australia*.

Spirakis C. S. (1981) The possible role of sulfate-reduction kinetics in the formation of hydrothermal uranium deposits. *Econ. Geol.* **76**, 2236–2239.

Taran Y. A., Varley N. R., Inguaggiato S. and Cienfuegos E. (2010) Geochemistry of H_2- and CH_4-enriched hydrothermal fluids of Socorro Island, Revillagigedo Archipelago, Mexico. Evidence for serpentinization and abiogenic methane. *Geofluids* **10**, 542–555.

Taylor S. D., Marcano M. C., Rosso K. M. and Becker U. (2015) An experimental and ab initio study on the abiotic reduction of uranyl by ferrous iron. *Geochim. Cosmochim. Acta* **150**, 154–172.

Wächtershäuser G. (1990) Evolution of the first metabolic cycles. *Proc. Natl. Acad. Sci. U.S.A.* **87**, 200–204.

Wächtershäuser G. (1993) The cradle chemistry of life – on the origin of natural-products in a pyrite-pulled chemoautotrophic origin of life. *Pure Appl. Chem.* **65**, 1343-134.

Wang A., Dhamenincourt P., Dubessy J., Guerard D., Landais P. and Lelaurain M. (1989) Characterization of graphite alteration in an uranium deposit by micro-Raman spectroscopy, X-ray diffraction, transmission electron microscopy and scanning electron microscopy. *Carbon* **27**, 209–218.

Wilde A. R., Mernagh T. P., Bloom M. S. and Hoffmann C. F. (1989) Fluid inclusion evidence on the origin of some Australian unconformity-related uranium deposits. *Econ. Geol.* **84**, 1627–1642.

Williams P. J., Barton M. D., Johnson D. A., Fontboté L., De Haller A., Mark G., Oliver N. H. S. and Marschik R. (2005) Iron oxide copper-gold deposits: geology, space-time distribution, and possible modes of origin. *Econ. Geol.*, 371–405.

Wolery T. J. (1992) EQ3/6, a software package for geochemical modeling of aqueous systems: package overview and installation guide (Version 7.0).

Yeo G. M. and Potter E. G. (2010) Review of reducing mechanisms potentially involved in the formation of unconformity-type uranium deposits and their relevance to exploration. In *Summary of Investigations 2010*, Volume 2. Saskatchewan Geological Survey. Paper A-12. 13p.

Associate editor: Gleb S. Pokrovski